Supporting Information

Comparing Fast Pressure Jump and Temperature Jump Protein Folding Experiments and Simulations

Anna Jean Wirth,[†] Yanxin Liu,[§] Maxim B. Prigozhin,[†] Klaus Schulten,[†‡§] and Martin Gruebele[†‡§]*

Department of Chemistry,[†] Center for Biophysics and Computational Biology,[‡] Department of Physics,[§] and Beckman Institute,[§] University of Illinois, Urbana, Illinois 61801, United States

Supplementary Methods

Sample preparation

FiP35 was expressed and purified as described previously,[1] although with a slightly different plasmid construction. Briefly, a construct encoding a fusion protein consisting of Glutathione-S-transferase (GST), a thrombin cleavage site, and FiP35 was cloned into pDream (GenScript). The fusion protein was expressed in BL21(DE3)-RIPL (Agilent) *E. coli* and captured and purified from the cell extract on an immobilized glutathione resin according to manufacturer's guidelines (GenScript). The protein was eluted by 10 mM glutathione in 50 mM Tris-HCl pH 8.0 and subsequently dialyzed against 10 mM sodium phosphate buffer.

FiP35 was cleaved from the purification tag by overnight incubation with biotinylated thrombin (EMD Millipore). Thrombin was removed by incubation with streptavidin-agarose resin (EMD Millipore) according to manufacturer's protocol. FiP35 was purified from cleaved GST via an ultrafiltration cell with 10 kDa cutoff membrane (Millipore). The purified FiP35 was lyophilized and resuspended to a final concentration of 200-400 μM FiP35 with 100 mM sodium phosphate buffer, pH 7.0.

Pressure thermodynamics

The thermodynamics of FiP35 unfolding under pressure were measured via fluorimeter (Cary Eclipse, Varian) in a pressure cell (ISS) as described previously.[2] The sample was placed in a quartz cuvette with a flexible cap to enable pressure transduction and inserted into the pressure cell. With a hydrostatic pressure generator (High Pressure Equipment Company), the cell was filled with spectroscopic grade ethanol (95.0 %, Acros organics) and pressurized up to 250 MPa with 4 minutes equilibration every 10 MPa increase or decrease. A custom built stage was used to mount the pressure cell into the fluorimeter.

Solutions of 50 or 100 μM FiP35 in 100 mM sodium phosphate buffer pH 7.0 and various concentrations of guanadinium hydrochloride (GuHCl) (Sigma) were assayed at room temperature. FiP35's single tryptophan was excited at 280 nm and emission was collected from 290 nm to 500 nm at each pressure. All thermodynamic traces showed complete reversibility (SI Figure 1). Additionally, FiP35 showed complete reversibilityup to 165 MPa (the maximum pressure in kinetics experiments) at 300 μM in 3M GuHCl, indicating that aggregation also does not occur with the higher concentrations used in kinetics experiments (SI Figure 2a).

Pressure denaturation traces at varying concentrations of GuHCl were analyzed using singular value decomposition (SVD). Because intensity is arbitrary across different pressure

titrations, the 2nd SVD vector (SVD2), which contains contributions from intensity and spectral shape change, was normalized by the 1st SVD vector (SVD1), which contains only intensity contributions. Plotting SVD2/SVD1 allows all of the pressure titrations to be analyzed together.

The unfolding traces were fit globally to a two-state unfolding model:

$$S(P) = \frac{S_u(P) + S_f(P)e^{-\Delta G(P,M)/RT}}{1 + e^{-\Delta G(P,M)/RT}}$$

where $S_u(P)$ and $S_f(P)$ are the linear folded and unfolded baselines, and the free energy of folding is given by:

$$\Delta G(P,M)_{u \to f} = \Delta V_{u \to f}(P - P_m) + g_m M$$

Here, $\Delta V_{U \to F}$ is the volume change of folding, P is pressure, P_m is the midpoint of the denaturation transition at 0 M GuHCl, g_m is a constant that describes the linear dependence of the free energy on GuHCl concentration, and M is the concentration of GuHCl.

Temperature thermodynamics

The thermodynamics of FiP35 unfolding under temperature were measured with a fluorimeter (Cary Eclipse, Varian) in an Agilent temperature controller. Tryptophan was excited at 280 nm and emission collected from 290 nm to 500 nm. Solutions of 10 μM FiP35 in 100 mM sodium phosphate buffer pH 7 and various concentrations of GuHCl were assayed and spectra were analyzed by SVD as described in the previous section. FiP35 has been shown previously to be reversible up to 90 °C at concentrations of up to 50 μM[1]. To verify that no aggregation occurs over the conditions assayed in kinetics, 300 μM FiP35 in 3M or 5M GuHCl was melted from 18-23 °C where it showed complete reversibility (SI figure 2b).

The temperature-probed unfolding traces were fit globally to a two-state model analogously to the pressure-probed thermodynamics:

$$S(T) = \frac{S_u(T) + S_f(T)e^{-\Delta G(T,M)/RT}}{1 + e^{-\Delta G(T,M)/RT}}$$

where $S_u(T)$ and $S_f(T)$ are the linear folded and unfolded baselines, and the free energy of folding is given by:

$$\Delta G(T,M)_{u \to f} = g_1(T - T_m) + g_m M$$

where g_1 is a constant describing the linear temperature dependence of the free energy, T is the temperature, T_m is the unfolding midpoint at 0 M GuHCl, g_m is a constant describing the linear dependence of the free energy on GuHCl concentration, and M is the GuHCl concentration.

Thermodynamic fit parameters are summarized in SI table 1. Due to FiP35's deviations from two-state behavior, fitted melting temperatures vary depending on how the fluorimeter data is analyzed. In this case, SVD2/SVD1 plotted versus temperature gives a melting temperature close to 90 °C. When the same data is expressed as an integrated fluorescent intensity versus temperature, as has been reported previously in the literature, the fitted melting temperature is 75 °C, consistent with previous measurements[1,3].

Pressure-jump kinetics

Pressure jump kinetics were measured as described previously[2,4] with a home-built fast pressure drop apparatus capable of pressure drops up to 250 MPa and kinetics resolution up to a microsecond. A solution of 300 μM FiP35 in 100 mM phosphate buffer pH 7.0 and various concentrations of GuHCl was placed into a hemispheric sample cavity machined on the face of a sapphire cube (Esco Products). Hydrostatic pressure was applied by a pressure generator (High

Pressure Equipment Company) through a pressure fitting to pressurize the sample, isolated from the pressurization fluid by a piece of mylar coated aluminum foil. A capacitor bank discharge delivered by a sharpened copper electrode burst a 0.007 inch thick stainless steel membrane, weakened by the applied pressure, dropping the sample from 165 MPa to atmospheric pressure in about a microsecond.

Tryptophan fluorescence lifetime decays were probed every 12.5 ns before, during, and after the jump by a mode-locked Ti:Sapphire laser (KMLabs) that was frequency-tripled to 280 nm with a commercial tripler (CSK Optronics). Tryptophan fluorescence was passed through a B370 band-pass filter, collected via a PMT (R7400U-03, Hamamatsu), and digitized by an oscilloscope (DPO7254) at a sampling period of 100 ps per point for 5 ms total data collection time. Two to three jumps were collected for each GuHCl concentration and, to improve signal to noise, 50 decays were binned in each jump before analysis.

Temperature-jump kinetics

Temperature jumps from 18°C to 23°C were carried out by a Surelite Q-switched Nd:YAG laser (Continuum) Raman-shifted to 1.9 μm and sent through a 50/50 beam splitter such that the sample is heated from two sides. The starting temperature was held constant by a temperature controller (Lake Shore 330, Lake Shore Cryotronics) and the size of the jump was measured by comparing the tryptophan decay at the end of the jump to tryptophan decays measured at equilibrium at various temperatures.

300 μM FiP35 in 100 mM sodium phosphate buffer pH 7.0 and varying concentrations of GuHCl samples or 200 μM tryptophan for jump calibration were held in fused silica cuvettes for the experiments. Tryptophan fluorescence was excited and collected as described in the previous section. 50 decays were binned in each jump before analysis, as in pressure-jump experiments.

Kinetic data analysis

The change in tryptophan lifetime reflects changes in the probed tryptophan's surrounding environment as the protein unfolds and is a more reliable observable than overall fluorescence intensity as it is immune to slight fluctuations in laser intensity. Chi analysis[5] is applied to quantify the change in lifetime over the course of the jump. The lifetime as a function of time, *S(t),* is decomposed into a linear combination of the lifetime before the jump, f_1, and the lifetime at the end of the jump, f_2, such that:

$$S(t) = c_1(t) f_1 + c_2(t) f_2$$

$\chi(t)$ is defined as the normalized $c_1(t)$:

$$\chi(t) = \frac{c_1(t)}{c_1(t) + c_2(t)}$$

c(t) thus ranges from 1 at the beginning of the jump to 0 at the end of the jump.

In T-jump experiments, a slow linear baseline due to photo-bleaching was fit and subtracted off. For P-jump experiments, portions of the kinetic traces with large amplitude random noise were removed and excluded entirely from analysis (see SI Figure 4). For both P-jump and T-jump experiments, the kinetic signal expressed as $\chi(t)$ was fit to a double-exponential :

$$\chi(t) = y_0 + A_1 e^{-t/\tau_1} + (1 - A_1) e^{-t/\tau_2}$$

For P-jump experiments, all replicates (2-3 jumps per GuHCl concentration) were fit to a double-exponential individually and the fitted parameters averaged together to get single values for A_1,

τ_1, and τ_2 for each GuHCl concentration. For T-jump experiments, two traces were binned together before each averaged pair was individually fit to double-exponentials.

Viscosity correction

The folding prefactor in the Arrhenius equation depends inversely on solvent viscosity and, consequently, the observed folding rate also shows viscosity dependence. High concentrations of GuHCl impart higher solvent viscosity, so observed folding rates from both pressure- and temperature-jump experiments were viscosity-corrected. Relative viscosities of GuHCl solutions to water,[6] ν_r, were used to correct for the folding rate decrease:[7]

$$k_{obs,corr} = \nu_r k_{obs}$$

In the main body figure 2a, the chevron plot does not have viscosity corrected rates in order to follow convention.

Chevron plots

Thermodynamic parameters from the global fits were used to calculate the free energy at the final equilibrium state after both temperature jumps and pressure jumps: 23°C, 0.1 MPa, and various GuHCl concentrations. The temperature-jump final state was chosen to match the final thermodynamic state after pressure jump. With the fitted observed folding rate, k_{obs}, from kinetics experiments, the approximate folding and unfolding rates (approximate because FiP35 is not a two-state folder) were calculated for each GuHCl concentration:

$$k_f = \frac{k_{obs} K_{eq}}{(1 + K_{eq})}$$

$$k_u = k_{obs} - k_f$$

where K_{eq} is given as:

$$K_{eq} = e^{-\Delta G / RT}$$

The thermodynamic parameters from the pressure-probed unfolding were used to calculate folding and unfolding rates for pressure jumps and those from the temperature-probed unfolding were used for temperature-jump calculations. However, at the equilibrium conditions (room temperature and atmospheric pressure), the folding free energies from the temperature and pressure probed thermodynamics were very close: -17 kJ/mol (temperature) *vs.* -16 kJ/mol (pressure).

Molecular Dynamics Simulations

Molecular dynamics simulations were performed in explicit solvent using the TIP3P water model[8] and the CHARMM22* force field for protein.[9] The CHARMM22* force field is a modified version of the widely used CHARMM22 force field with CMAP corrections.[10-12] It has been employed successfully to simulate folding of a wide range of fast folding proteins with both α-helical and β-sheet native topology.[13] The structure of the WW domain (FiP35 mutant, residues 4 to 38) from the protein data bank (PDB code 2F21)[14] was placed in a cubic box of 10,232 water molecules and neutralized with 6 sodium ions and 9 chloride ions employing VMD.[15] The simulated systems, including protein, water molecules, and ions, measured 68.4 Å

in each dimension at T = 325 K and P = 0.1 MPa and contained 31,273 atoms. All simulations were carried out with periodic boundary conditions in a constant particle number, temperature, and pressure ensemble (NPT). Starting from the native state of the protein, two types of simulations were performed: pressure jump and temperature jump. In both cases, the simulations started with 100 ns equilibrium simulation of the native state and ended with multi-microseconds refolding simulation, both at T = 325 K and P = 0.1 MPa. The temperature for ambient conditions, 325 K, was chosen because it is well below FiP35's melting temperature and directly comparable to previous P-jump simulations.[2,16] The difference between the simulation types lies in the denaturing procedure which followed the 100-ns equilibrium simulation. In a pressure-jump simulation, pressure was increased from 0.1 MPa to 900 MPa in 0.3 μs at a rate of 0.9 MPa/300 ps, followed by a 1-μs high-pressure equilibrium simulation (P = 900 MPa) and a pressure-drop simulation in which pressure was jumped downward from 900 MPa to 0.1 MPa in 0.3 μs at a rate of -0.9 MPa/300 ps. The temperature was maintained at T = 325 K through the pressure-jump simulation. In a temperature-jump simulation, the pressure was maintained at P = 0.1 MPa throughout the simulation and the system was heated up to 400 K for 1 μs between the initial 100-ns equilibrium simulation and the final refolding simulation, both at T = 325 K. To generate multiple refolding trajectories, the pressure or temperature unfolded state was equilibrated for an additional 200 ns respectively, during which the structures were taken at t = 0 ns, 100 ns, and 200 ns to continues the P-jump and T-jump simulations at ambient conditions.

Molecular dynamics simulations using NAMD

The simulation algorithm and features of the NAMD program are described previously.[17] The systems to be simulated were first subjected to 3000 steps of conjugate gradient minimization and equilibrated for 300 ps with harmonic restraints applied to all the heavy atoms of the protein. The simulation was then continued for 3 ns without restraints at a constant pressure of 0.1 MPa using Nosé -Hoover Langevin piston barostat and at a constant temperature of 325 K with Langevin damping constant of 5.0 ps^{-1} . In the subsequent simulations, constant temperature was maintained using Langevin dynamics with a damping constant of 1.0 ps^{-1} and multiple time stepping employed with an integration time step of 2.0 fs, short-range forces being evaluated every time step and long-range electrostatics evaluated every three time steps. All bonds involving hydrogen in the protein were constrained using RATTLE,[18] while the geometries of water molecules were maintained using SETTLE.[19]

Cutoff for short-range nonbonded interactions was 8.0 Å with shifting beginning at 7.0 Å; long-range electrostatics was calculated using the particle-mesh Ewald method.[20] The cutoff was chosen to accelerate the simulation on general purpose supercomputers while maintaining a sufficient level of accuracy. Indeed, it is accurate enough to fold two fast folding proteins: villin headpiece[21] and lambda repressor.[22]

Molecular dynamics simulations on Anton

The refolding simulations were carried out on the Anton platform.[23,24] Multiple time stepping was employed, with an integration time step of 2.0 fs. The Multigrator integration procedure was employed.[25] Short-range forces were evaluated every time step and long-range electrostatics every three time steps. Cutoff for the short-range nonbonded interactions was 14.18 Å, as recommended by the developers of the Anton machine at DE Shaw Research. Long-range electrostatics were calculated using the k-Gaussian Split Ewald method[26] with a 32 × 32 × 32

grid to better suit the Anton machine. All bonds involving hydrogen atoms were constrained using SHAKE.[27]

Bayesian rate analysis

Using a Bayesian analysis approach,[28] the rate of formation for the loop 1 and loop 2 intermediate and the folding rate from each of the intermediates were estimated from the P-jump MD simulations. Briefly, Bayes rule states that the probability of a model corresponding to a given data set, or the posterior probability density, can be derived from the probability of the model to generate the given data. The posterior probability density depends on the prior probability density or the state of knowledge about the model given previous data. Taking a uniform distribution as the prior probability density (or assuming no prior knowledge of the model) and specifically treating a two-state transition model, the probability that the two state kinetic model with rate k corresponds to the molecular dynamics data set is given by:

$$p_U(k \mid D,X,I) = \frac{\theta^{n+1}}{n!} k^n \exp[-k\theta]$$

where θ is the total simulation time, n is the number of simulations where a folding transition occurred, and k is the rate. The total simulation time is calculated by summing the time to the folding transition in each simulation. For simulations where no transition occurred, the folding time is the length of the simulation. The expectation value and variance of the distribution are:

$$\langle k \rangle_U = \frac{n+1}{\theta}, \mathrm{var}(k)_U = \frac{n+1}{\theta^2}$$

The total folding times, values of n, and calculated rates and variance are summarized in SI table 4. To calculate the overall folding time for the pressure and temperature jump simulations, FiP35's folding to the native state is approximated as a two-state transition. For the pressure jump simulations, the forward folding rates to the two intermediates and from the intermediates to the native state were calculated by approximating each of the intermediate forming transitions and the intermediate to native state transitions as separate two-state reactions. To calculate the rate of formation for the loop 1 intermediate, the number of observed transitions was 2 and the total folding time was given as the sum of the loop 1 intermediate formation times in two simulations and the entire simulation time for the simulation where the loop 2 intermediate occurred. The rate of the loop 2 intermediate was calculated analogously but with the number of observed transitions as 1.

To calculate the formation of the native state from the intermediates, the simulations were treated as beginning at the first appearance of the intermediate structure. There is, thus, is just 1 simulation that shows the loop 2 intermediate to native state transition with its total folding time given as the time to formation of the native state. The loop 1 intermediate to native state transition is observed in two simulations with the total folding time given as the sum of the intermediate to native folding times in those two simulations.

Kinetic modeling

To assess whether the rates and models observed in the pressure-jump simulations were consistent with experimental data, we performed kinetic simulations. Several kinetic models were solved populated with transition rates from the MD simulations (calculated as described in the previous section) by numerically solving the differential rate equations. The time depended of the concentration of each species was simulated for 100 μs with a time resolution of 0.01 μs.

Various signal functions were also tested. Because the tryptophan residue of FiP35 is located between strand 1 and strand 2, it is reasonable to assume that all measureable signal in our experiment arises from the formation of the loop 1 intermediate or the native state. Thus, signal functions of the following form were evaluated:

$$S(t) = c_{IL1}[I_{L1}](t) + c_N[N](t)$$

where $[I_{L1}]$ and [N] are the time dependent concentrations of the loop 1 intermediate and the native state, respectively. Their coefficients, C_{IL1} and C_N, were varied from 0 to 1 in intervals of .01 such that:

$$c_{IL1} + c_N = 1$$

To test model and signal function combinations, each signal function was compared to experimentally generated data. To account for the disparity between simulated folding rates and experimental folding rates, the simulated data was scaled. To determine the scaling factor, the previously determined *in silico* folding rate of FiP35 on the Anton computer[29] was compared to the experimentally determined FiP35 folding rate at the same temperature.[1] As our simulations were performed with the same force field on the same super-computer as the previous *in silico* studies, this calculation should provide a robust link between simulation and experimental time-scales. In previous simulations,[29] FiP35 gave a folding time of 10 μs at the *in silico* melting temperature. At the experimentally determined melting temperature, ~44 K below the *in silico* melting temperature, FiP35 folds in 27 μs.[1] This gives a scaling factor of 2.7, in relatively close agreement with the 2.1 scaling factor necessary to account for the lessened viscosity of the TIP3 water model.[30]

Since the P-jump experiment is carried under conditions strongly favoring the native state, our kinetic simulation assumes reverse rates are negligible. To account for the decrease in rate due to perturbation of the energy landscape by GuHCl as well as the change in solution viscosity at high concentrations of GuHCl, the simulation was further scaled for comparison to experiment. In this case, the scaling factor was obtained by taking the ratio of the rate from the 0 M GuHCl pressure jump experiment and the viscosity uncorrected rate from the 5 M GuHCl jumps. This yielded a scaling factor of 38.7.

To assess each model and the various signal functions for each model, each simulated kinetic trace was fit to a double exponential. The fitted fast phase amplitude, fast phase rate, and slow phase rate were compared to those obtained from experiment via a scoring function:

$$Score = \sqrt{\left(\frac{k_{fast,obs} - k_{fast,sim}}{k_{fast,obs}}\right)^2 + \left(\frac{k_{slow,obs} - k_{slow,sim}}{k_{slow,obs}}\right)^2 + \left(\frac{A_{fast,obs} - A_{fast,sim}}{A_{fast,obs}}\right)^2}$$

The lowest scoring signal functions were used to report each model's closeness to experiment.

SI Figure 11 summarizes all of the tested kinetic models. Each model and the details of its simulation are summarized below.

I: Heterogeneous transition state model

Phi-value analysis has shown that WW-domains can fold through two transition states with either loop 1 or loop 2 formed.[31] In this kinetic model, FiP35 would fold through either of these two transition states through parallel paths (SI Figure 11). Our molecular dynamics simulations imply that this model is unlikely because, particularly in the case of the loop 2 formed structure, we observe persistence of the partially folded structures in MD simulations.

Because this model has no intermediates, the change in concentration of the native state was used as the signal function:

$$S(t) = [N](t)$$

As expected, the model did not closely match experiment giving a score of 29. The fitted values for the simulated data are summarized in SI table 5.

II: Folding through the loop 2 intermediate

In this model, FiP35 folds through a stable loop 2 intermediate and through a parallel path to the native state with no intermediate (SI Figure 11). As in the two transition-state model, the signal function was given by the change in concentration of the native state. Because of the similarity of the signal functions, this gives very similar results to the two transition state model. The double exponential kinetics yielded by the simulation were a poor fit to the experimental data giving a score of 29. The fitted values for the simulated data are summarized in SI table 5.

III: Folding through the loop 1 intermediate

In this model, FiP35 folds through a loop 1 intermediate and through an alternate path to the native state with no intermediate (SI Figure 11). In this case, the signal function was given as a linear combination of the concentration of the native state and the loop 1 intermediate:

$$S(t) = c_{IL1}[I_{L1}](t) + c_N[N](t)$$

The scores for each tested signal function are shown graphically in SI Figure 12 The minimum score occurred for a signal function with c_{IL1}=0.94 giving a score of 0.14. The fitted parameters for the kinetics were thus a close match for the experimental kinetics and are shown in SI table 5.

While this model provides an excellent fit to experimentally observed kinetics, it deviates substantially from the observed mechanism in MD simulations. In the simulations, one trajectory shows a stable loop 2 intermediate, which persists for several microseconds while the loop 1 intermediate is far more transient in the other two trajectories. This model is not consistent with this data because it designates the most transient of observed structures an intermediate while the more stable observed structure a transition state.

IV: Folding through both the loop 1 and loop 2 intermediate

In this model, FiP35 folds through a loop 1 intermediate and through a parallel path to the native state through a loop 2 intermediate (SI Figure 11). As in case III, the signal function was comprised of contributions of both the native state and the loop 1 intermediate. The scores for each tested signal function are shown graphically in SI Figure 12. The minimum score occurred for a signal function with c_{IL1}=0.95 giving a score of 0.15. This model is thus consistent with experimental data and also reflects the observed folding mechanism in MD simulation.

Sequence comparison between hairpin 1 and hairpin 2

In peptides structured similarly to FiP35, the degree of partitioning between a loop 1-first and loop 2-first folding mechanism was correlated to the degree of sequence similarity between the two hairpins: the more similar the sequence, the more evenly partitioned the folding was between the two pathways.[32] We calculated the sequence similarity between hairpin 1 and hairpin 2 for FiP35. Hairpin 1 is defined as residues 11-26 and hairpin 2 as residues 22-33. Because strand 2 is shared between hairpin 1 and hairpin 2, we used hydrogen bonding patterns to determine which residues in strand 2 interacted most with strand 1 or strand 3. SI figure 13 shows the hydrogen bonding pattern for FiP35. Residues that form backbone hydrogen bonds with strand 1 were assigned to hairpin 2 (because their side changes interact with strand 3) and vice versa. Residues from strand 2 that formed no hydrogen bonds were shared between the two hairpins.

Sequences of the individual hairpins were aligned by overlapping the two loop regions. As the loops are different lengths, this gives two possible alignments: alignment 1, where V22 of

hairpin 2 overlaps with E12 of hairpin 1, and alignment 2 where V22 of hairpin 2 overlaps with W11 of hairpin 1. Residues were tested pair-wise for sequence similarity (polar, hydrophobic, or charged) or sequence identity. Sequence similarity was calculated as the number of similar residues normalized by the average length of the two hairpins. Neither alignment had any sequence identity while alignment 1 had 36% sequence similarity and alignment 2 14% sequence similarity.

SI Table 1: Thermodynamics. Values are derived from global fits and errors are fit uncertainties.

	g_1 or $\Delta V_{u \rightarrow f}$	T_m or P_m	g_m (kJ mol^{-1} M^{-1})
Pressure	3.00 ± 0.25 mL mol^{-1}	677.0 ± 34 MPa	3.783 ± 0.16
Temperature	0.3039 ± 0.0068 kJ mol^{-1} K^{-1}	362.7 ± 0.44 K	3.265 ± 0.11

SI Table 2: Pressure-jump kinetics. Errors are standard error (standard deviation of the mean).

[GuHCl] (M)	$\%A_1$	τ_1 (μs)	τ_1 (μs), viscosity corrected	τ_2 (μs)	τ_2 (μs), viscosity corrected
2.5	34.1 ± 0.9	12.7 ± 7.7	11.3 ± 6.8	218 ± 54	193 ± 48
3	50.8 ± 5.2	13.6 ± 3.0	11.6 ± 2.6	398 ± 42	340 ± 36
4	32.6 ± 3.6	22.2 ± 6.0	17.4 ± 4.7	452 ± 24	355 ± 19
5	47.3 ± 3.3	30.0 ± 4.4	21.2 ± 3.1	727 ± 69	513 ± 48

SI Table 3: Temperature-jump kinetics. Errors are standard error.

[GuHCl] (M)	$\%A_1$	τ_1 (μs)	τ_1 (μs), viscosity corrected	τ_2 (μs)	τ_2 (μs), viscosity corrected
3	77.7 ± 1.0	7.52 ± .78	6.42 ± .64	276 ± 21	235 ± 18
3.5	68.6 ± 1.1	7.48 ± .36	6.14 ± .29	269 ± 11	221 ± 9.0
4	59.2 ± 1.3	7.07 ± .69	5.55 ± .54	310 ± 18	244 ± 14
4.5	50.7 ± 1.1	8.70 ± .51	6.50 ± .38	368 ± 12	275 ± 8.9
5	49.8 ± 1.0	8.68 ± .43	6.13 ± .30	427 ± 7.5	302 ± 5.3

SI table 4. Rates from Bayesian analysis.

Transition	n	Θ (μs)	$\langle k \rangle_U$ (μs)$^{-1}$
U → F, temperature	2	33.8	0.0895 ± 0.052
U → F, pressure	3	33.5	0.119 ± 0.059
U → I_{L1}, pressure	2	30.7	0.0978 ± 0.056
U → I_{L2}, pressure	1	30.7	0.0652 ± 0.046
I_{L1} → F, pressure	2	0.940	3.19 ± 1.8
I_{L2} → F, pressure	1	1.88	1.06 ± 0.75

SI table 5. Simulation summary. Rates shown are from the double exponential fits to the signal functions that most closely match experiment for each model. Amplitude shown is percent of the fitted amplitude that corresponds to the fast phase. The percentage of the loop 1 intermediate refers to the composition of the signal function that best matched the experimental data where the percentage of the signal function corresponding to the native state is given by 100-$\%I_{loop\ 1}$.

Model	τ_{fast} (μs)	τ_{slow} (μs)	$\%A_{fast}$	$\%I_{loop\ 1}$
II: parallel transition states	1	671	2.4 x 10^{-10}	0
III: loop 2 intermediate	1	671	2.4 x 10^{-10}	0
IV: loop 1 intermediate	32.7	666	47	94
V: two parallel intermediates	29.3	654	52	95

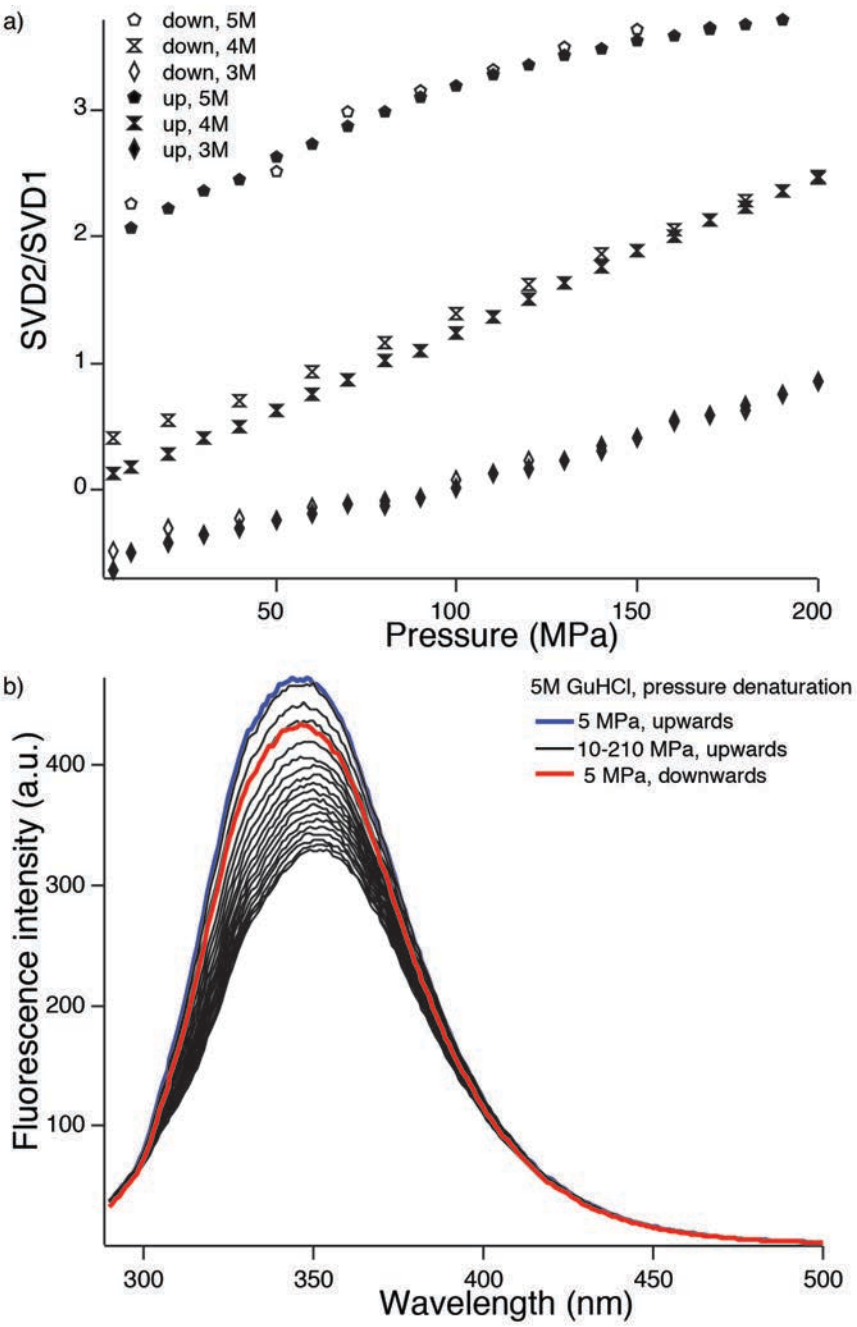

SI Figure 1. Pressure thermodynamics reversibility. a) High GuHCl concentration unfolding traces (closed markers) expressed as the ratio of SVD2 to SVD1 with refolding traces (open markers). Only high concentration GuHCl traces are shown because significant unfolding occurred at these concentrations. b) Fluorescence spectra of the 5M GuHCl unfolding trace. First unfolding (dark blue) and last refolding (red) trace are highlighted for comparison. The small difference in intensity between red and blue traces is due to intensity fluctuations that occur from pressurization and depressurization of the cell. SVD2/SVD1 shows nearly complete reversibility because it reflects wavelength shift (intensity component is normalized out).

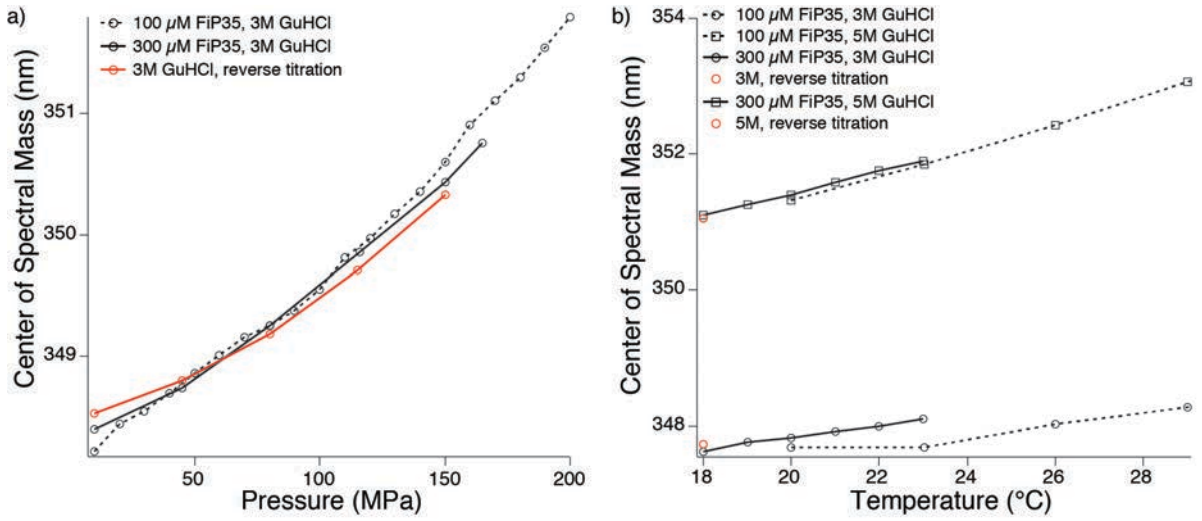

SI Figure 2. FiP35 reversibility at 300 μM a) Upwards (solid black line) and reverse (red line) pressure titration of 300μM FiP35 in 3M GuHCl plotted with a pressure titration of 100 μM FiP35 in 3M GuHCl (dashed black line). No concentration dependence of the thermodynamics are observed and the high concentration titration shows complete reversibility. b) Upwards (solid black lines) and reverse (red points) temperature titration of 300 μM FiP35 in 3M (circles) or 5M (squares) GuHCl plotted with corresponding temperature titrations at 10 μM FiP35 (dashed lines). No concentration dependence of the thermodynamics are observed at the low temperatures assayed in kinetics experiments, 18 to 23 °C, and the high concentration titrations show complete reversibility.

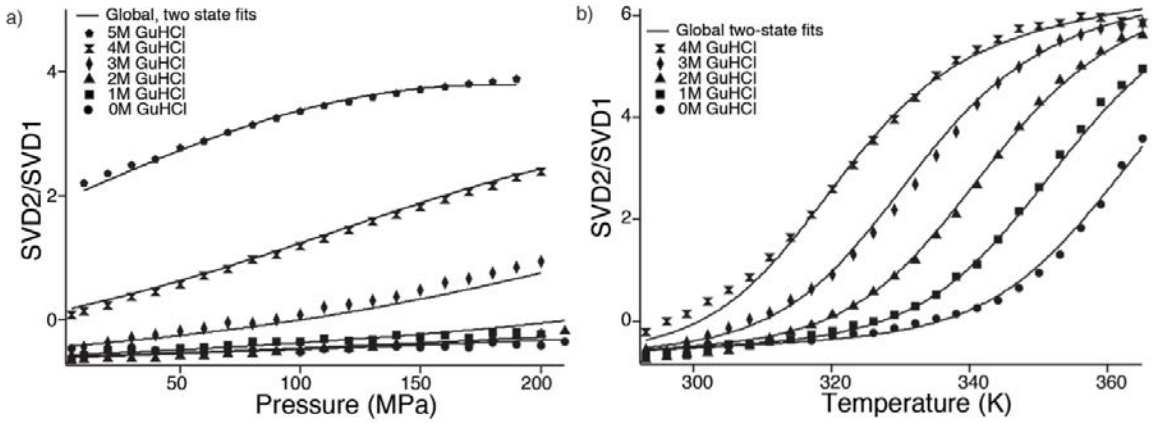

SI Figure 3. Pressure and temperature thermodynamics with global fits. Y-axis is the ratio of component 2 and 1 from the singular value decomposition (SVD), which corresponds to mean wavelength shift.

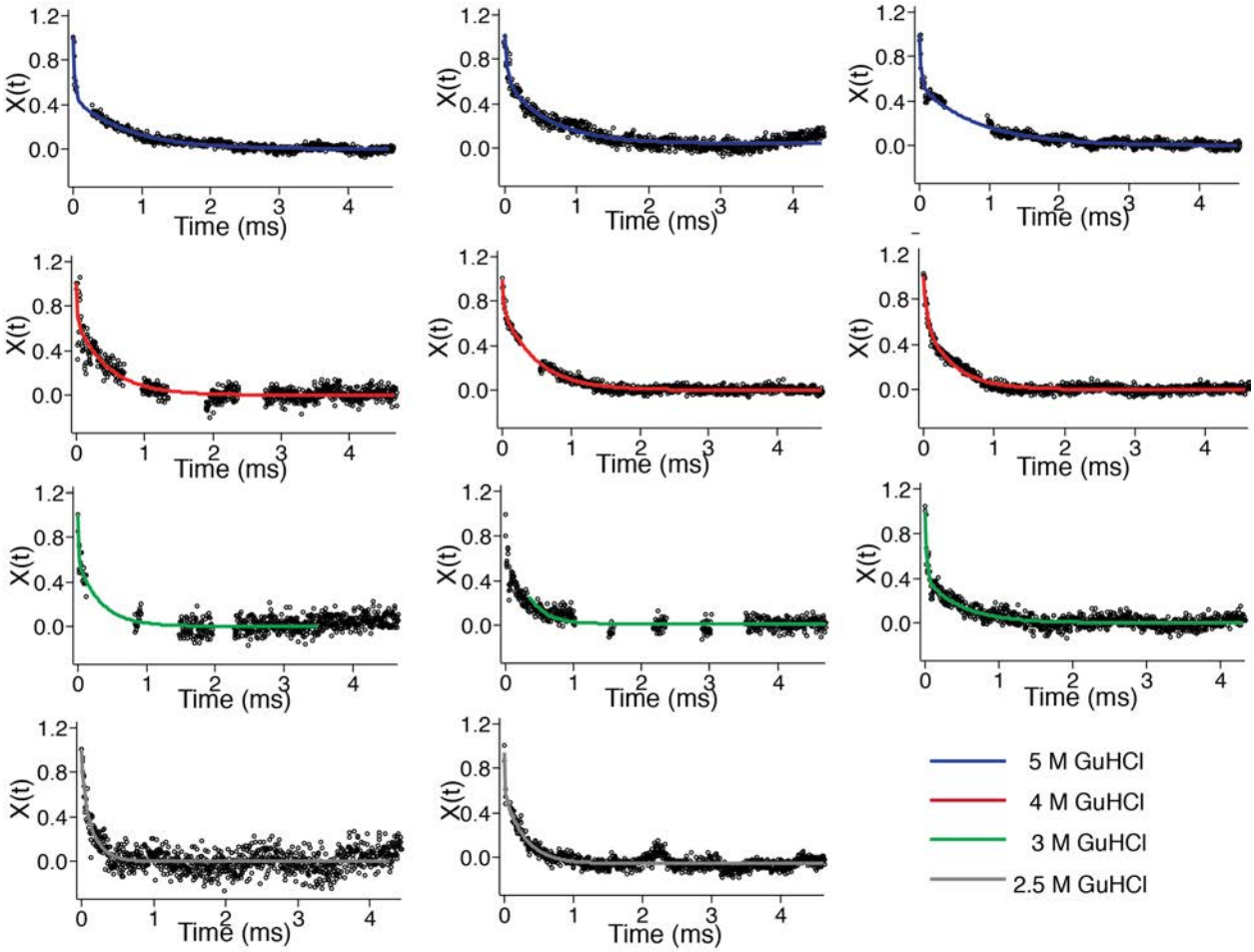

SI Figure 4. Pressure-jump kinetics. Data is smoothed and each data point corresponds to 5 μs. Fits are double-exponential. Gaps in the kinetic traces correspond to regions of high noise that were excluded from analysis, but each GuHCl concentration has one trace with no gaps.

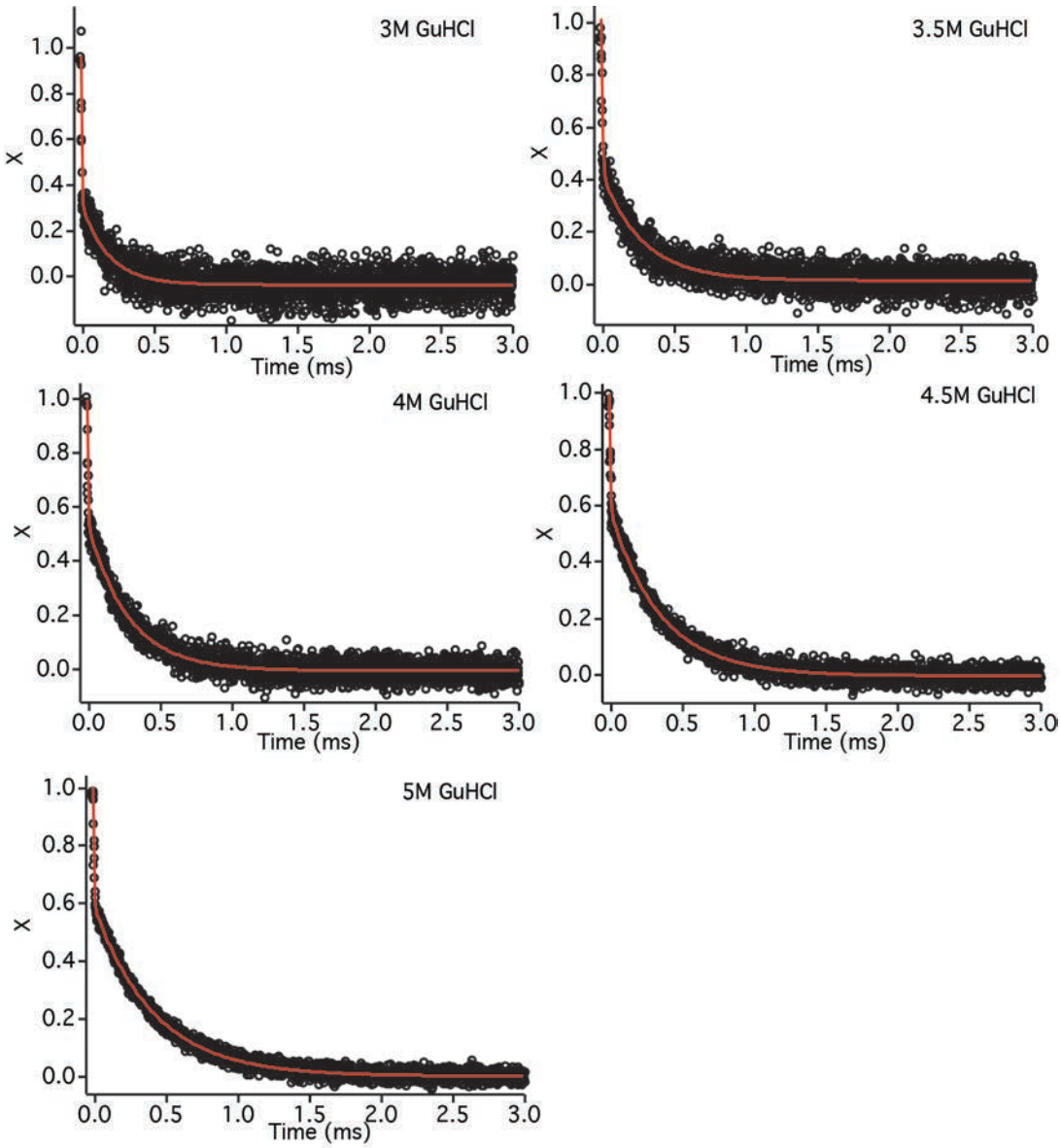

SI Figure 5. Temperature-jump kinetics. Double-exponential fits are shown in red. Traces and fits shown are averages over all collected traces (50). Each data point corresponds to 1.25 μs. Only 3 ms of data were analyzed to avoid cooling effects at long timescales. A slow linear baseline corresponding to irreversible photobleaching has been removed from all traces.

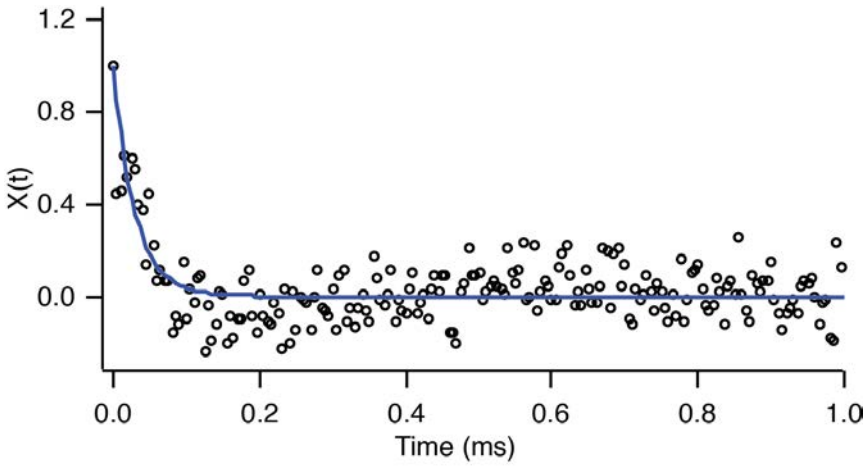

SI Figure 6. Pressure-jump kinetics at 0 M GuHCl. Data is smoothed and each data point corresponds to 5 μs. The extremely small population of proteins undergoing transition makes the signal-to-noise ratio very low and only a single exponential phase can be fit with reasonable certainty. The blue line represents a single-exponential fit with observed time constant of 29.5 ± 1 μs (error is fit uncertainty).

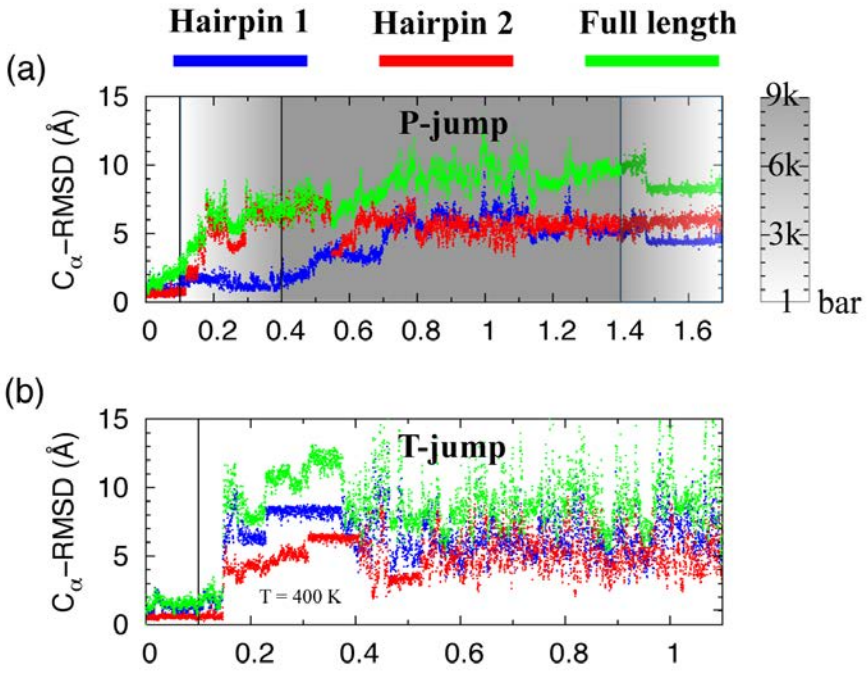

SI Figure 7. Structural characterization of the FiP35 unfolding trajectories. Time is in μs. (a) Pressure-jump unfolding simulation. (b) Temperature-jump unfolding simulation. Cα-RMSD values have been calculated relative to the crystal structure 2F21.[14] The pressure is shown as the color background, which varies from 1 bar (white) to 9 kbar (dark gray). Hairpin 1 contains residues 11 to 25 and hairpin 2 contains residues 22 to 33. The full length Cα-RMSD are calculated using residues 7 to 35.

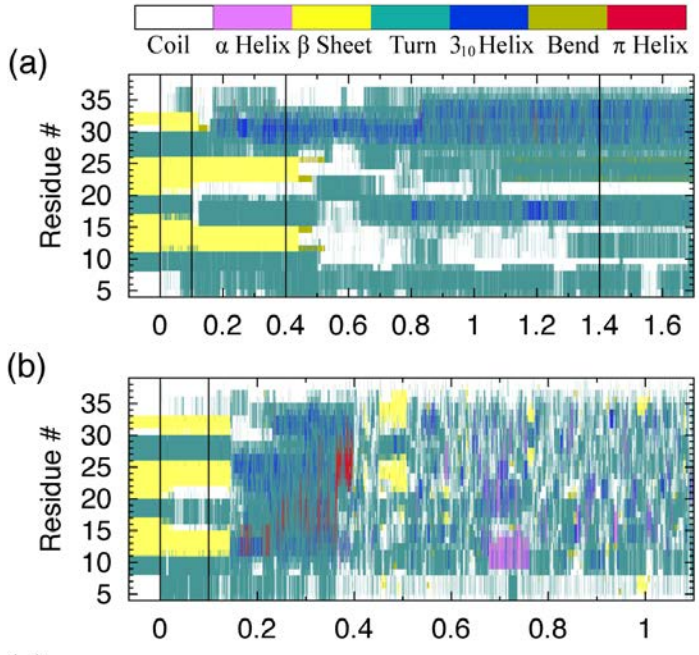

SI Figure 8. Time evolution of the secondary structure throughout the unfolding trajectories. Time is in μs. (a) Pressure-jump unfolding simulation. (b) Temperature-jump unfolding simulation. The secondary structure of the crystal structure is shown on the left.

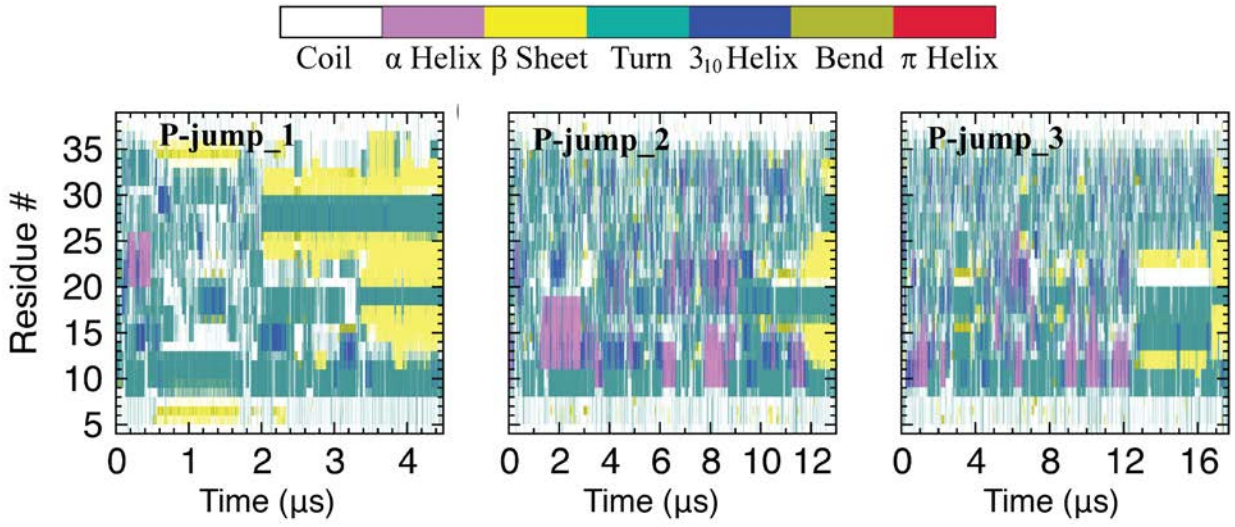

SI Figure 9. Time evolution of the secondary structure for the pressure-jump refolding.

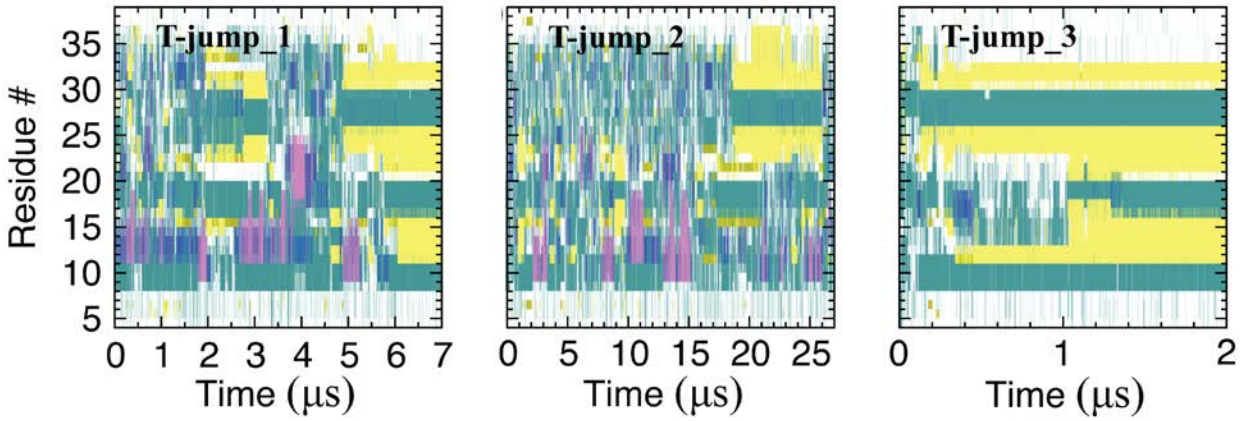

SI Figure 10: Time evolution of the secondary structure for the temperature-jump refolding trajectories. Secondary structure is as defined in SI Figure 9.

Model	Model score	Assessment
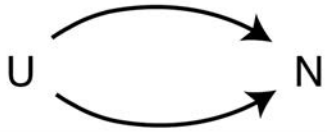	29	Simulation poorly matches experimental data.
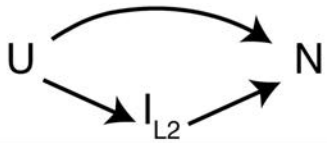	29	Simulation poorly matches experimental data.
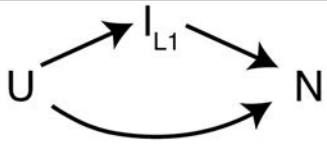	.14	Simulation matches experimental data, but a long lived loop 2 intermediate was observed in MD data.
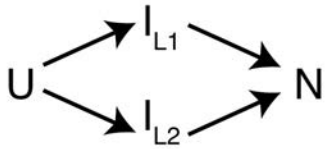	.15	Simulation matches experimental data and model matches intermediates observed in MD data.

SI Figure 11. Summary of tested kinetic models and outcomes.

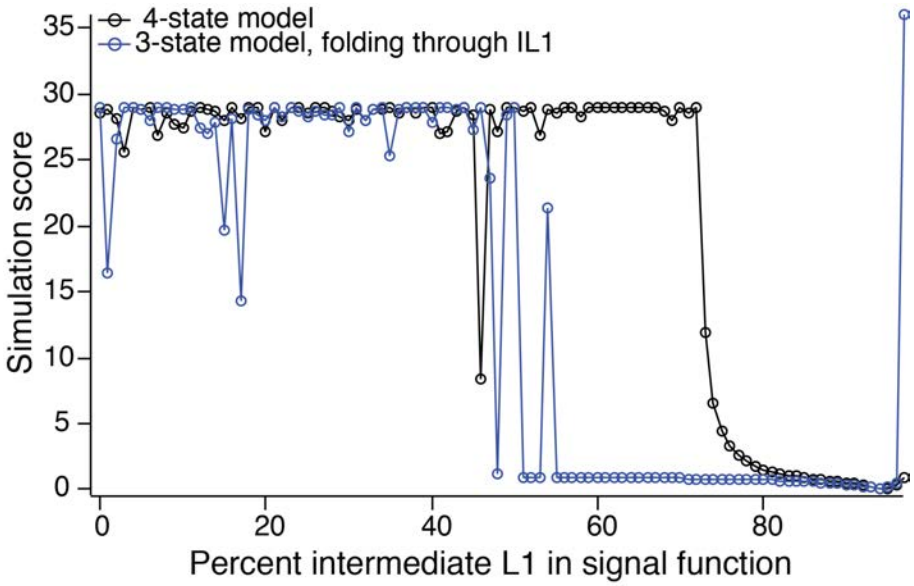

SI Figure 12. Score (describing distance between simulated kinetics and experimental kinetics) of all tested signal functions for the two best kinetic models. A low score indicates a closer match to experimental data. Signal function is represented on x-axis by percentage of the signal function corresponding to the loop 1 intermediate.

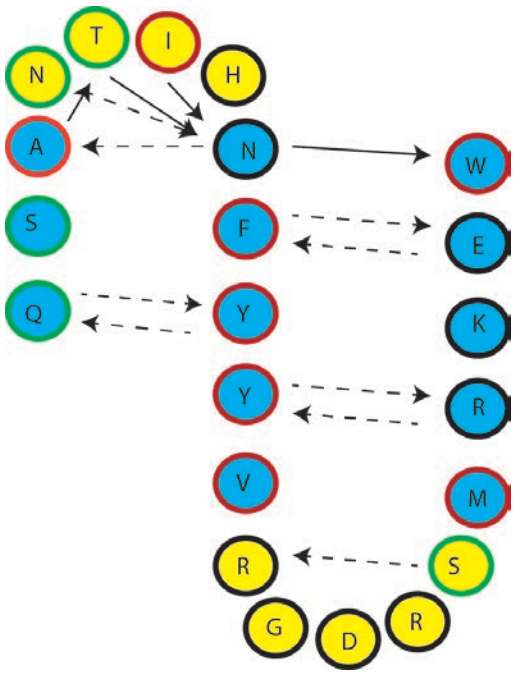

SI Figure 13. Hydrogen bonding patterns in Fip35.[31] In this schematic N-terminus is on the right and the C-terminus is on the left (strand ordering from left to right is 3-1). Blue circles indicate strand amino acids while yellow are loop. Colored ring around amino acids is color coded for type: green is polar, black is charged, and red is hydrophobic. Hydrogen bonding is indicated by arrows where dashed arrows indicate backbone-backbone bonding and solid arrows indicate backbone-side chain bonding.

Supplementary References

(1) Liu, F.; Nakaema, M.; Gruebele, M. *J. Chem. Phys.* **2009**, *131*, 9.

(2) Prigozhin, M. B.; Liu, Y. X.; Wirth, A. J.; Kapoor, S.; Winter, R.; Schulten, K.; Gruebele, M. *Proc. Natl. Acad. Sci. USA* **2013**, *110*, 8087.

(3) Liu, F.; Du, D. G.; Fuller, A. A.; Davoren, J. E.; Wipf, P.; Kelly, J. W.; Gruebele, M. *Proc. Natl. Acad. Sci. USA* **2008**, *105*, 2369.

(4) Dumont, C.; Emilsson, T.; Gruebele, M. *Nat. Methods* **2009**, *6*, 515.

(5) Ervin, J.; Sabelko, J.; Gruebele, M. *J. Photochem. Photobiol. B* **2000**, *54*, 1.

(6) Kawahara, K.; Tanford, C. *J. Biol. Chem.* **1966**, *241*, 3228.

(7) Denos, S.; Dhar, A.; Gruebele, M. *Faraday Discuss.* **2012**, *157*, 451.

(8) Jorgensen, W. L.; Chandrasekhar, J.; Madura, J. D.; Impey, R. W.; Klein, M. L. *J. Chem. Phys.* **1983**, *79*, 926.

(9) Piana, S.; Lindorff-Larsen, K.; Shaw, D. E. *Biophys. J.* **2011**, *100*, L47.

(10) MacKerell, A. D.; Bashford, D.; Bellott, M.; Dunbrack, R. L.; Evanseck, J. D.; Field, M. J.; Fischer, S.; Gao, J.; Guo, H.; Ha, S.; Joseph-McCarthy, D.; Kuchnir, L.; Kuczera, K.; Lau, F. T. K.; Mattos, C.; Michnick, S.; Ngo, T.; Nguyen, D. T.; Prodhom, B.; Reiher, W. E.; Roux, B.; Schlenkrich, M.; Smith, J. C.; Stote, R.; Straub, J.; Watanabe, M.; Wiorkiewicz-Kuczera, J.; Yin, D.; Karplus, M. *J Phys Chem B* **1998**, *102*, 3586.

(11) Mackerell, A. D.; Feig, M.; Brooks, C. L. *J Comput Chem* **2004**, *25*, 1400.

(12) MacKerell, A. D.; Feig, M.; Brooks, C. L. *J Am Chem Soc* **2004**, *126*, 698.

(13) Lindorff-Larsen, K.; Piana, S.; Dror, R. O.; Shaw, D. E. *Science* **2011**, *334*, 517.

(14) Jager, M.; Zhang, Y.; Bieschke, J.; Nguyen, H.; Dendle, M.; Bowman, M. E.; Noel, J. P.; Gruebele, M.; Kelly, J. W. *Proc. Natl. Acad. Sci. U. S. A.* **2006**, *103*, 10648.

(15) Humphrey, W.; Dalke, A.; Schulten, K. *J. Mol. Graph. Model* **1996**, *14*, 33.

(16) Liu, Y. X.; Prigozhin, M. B.; Schulten, K.; Gruebele, M. *J. Am. Chem. Soc.* **2014**, *136*, 4265.

(17) Phillips, J. C.; Braun, R.; Wang, W.; Gumbart, J.; Tajkhorshid, E.; Villa, E.; Chipot, C.; Skeel, R. D.; Kale, L.; Schulten, K. *J. Comput. Chem.* **2005**, *26*, 1781.

(18) Andersen, H. C. *J Comput Phys* **1983**, *52*, 24.

(19) Miyamoto, S.; Kollman, P. A. *J Comput Chem* **1992**, *13*, 952.

(20) Darden, T.; York, D.; Pedersen, L. *J. Chem. Phys.* **1993**, *98*, 10089.

(21) Freddolino, P. L.; Schulten, K. *Biophys J* **2009**, *97*, 2338.

(22) Liu, Y. X.; Strumpfer, J.; Freddolino, P. L.; Gruebele, M.; Schulten, K. *J Phys Chem Lett* **2012**, *3*, 1117.

(23) Shaw, D. E.; Deneroff, M. M.; Dror, R. O.; Kuskin, J. S.; Larson, R. H.; Salmon, J. K.; Young, C.; Batson, B.; Bowers, K. J.; Chao, J. C.; Eastwood, M. P.; Gagliardo, J.; Grossman, J. P.; Ho, C. R.; Ierardi, D. J.; Kolossvary, I.; Klepeis, J. L.; Layman, T.; Mcleavey, C.; Moraes, M. A.; Mueller, R.; Priest, E. C.; Shan, Y. B.; Spengler, J.; Theobald, M.; Towles, B.; Wang, S. C. *Commun. Acm.* **2008**, *51*, 91.

(24) Shaw, D. E.; Dror, R. O.; Salmon, J. K.; Grossman, J. P.; Mackenzie, K. M.; Bank, J. A.; Young, C.; Deneroff, M. M.; Batson, B.; Bowers, K. J.; Chow, E.; Eastwood, M. P.; Ierardi, D. J.; Klepeis, J. L.; Kuskin, J. S.; Larson, R. H.; Lindorff-Larsen, K.; Maragakis, P.; Moraes, M. A.; Piana, S.; Shan, Y. B.; Towles, B. In *Proc. Conf. High Perf. Comp. Net. Stor. Anal.* 2010.

(25) Lippert, R. A.; Predescu, C.; Ierardi, D. J.; Mackenzie, K. M.; Eastwood, M. P.; Dror, R. O.; Shaw, D. E. *J. Chem. Phys.* **2013**, *139*.

(26) Shan, Y. B.; Klepeis, J. L.; Eastwood, M. P.; Dror, R. O.; Shaw, D. E. *J. Chem. Phys.* **2005**, *122*.

(27) Ryckaert, J. P.; Ciccotti, G.; Berendsen, H. J. C. *J Comput Phys* **1977**, *23*, 327.

(28) Ensign, D. L.; Pande, V. S. *J. Phys. Chem. B.* **2009**, *113*, 12410.

(29) Shaw, D. E.; Maragakis, P.; Lindorff-Larsen, K.; Piana, S.; Dror, R. O.; Eastwood, M. P.; Bank, J. A.; Jumper, J. M.; Salmon, J. K.; Shan, Y. B.; Wriggers, W. *Science* **2010**, *330*, 341.

(30) Mark, P.; Nilsson, L. *J. Phys. Chem. B.* **2001**, *105*, 24A.

(31) Jager, M.; Nguyen, H.; Crane, J. C.; Kelly, J. W.; Gruebele, M. *J Mol Biol* **2001**, *311*, 373.

(32) Ferrara, P.; Caflisch, A. *J Mol Biol* **2001**, *306*, 837.